Article

Enhancing the Effectiveness of Oxygen Evolution Reaction by Electrodeposition of Transition Metal Nanoparticles on Nickel Foam Material

Mateusz Łuba [1] , Tomasz Mikołajczyk [1,*] , Mateusz Kuczyński [1], Bogusław Pierożyński [1,*] and Ireneusz M. Kowalski [2]

[1] Department of Chemistry, Faculty of Agriculture and Forestry, University of Warmia and Mazury in Olsztyn, Plac Lodzki 4, 10-727 Olsztyn, Poland; mateusz.luba@uwm.edu.pl (M.Ł.); mateusz.kuczynski@uwm.edu.pl (M.K.)

[2] Department of Rehabilitation, Faculty of Medical Sciences, University of Warmia and Mazury in Olsztyn, Zolnierska 14C Street, 10-561 Olsztyn, Poland; rehab@uwm.edu.pl

* Correspondence: tomasz.mikolajczyk@uwm.edu.pl (T.M.); bogpierozynski@yahoo.ca (B.P.); Tel.: +48-89-523-4177 (B.P.)

Abstract: Electrochemical oxygen evolution reaction (OER) activity was studied on nickel foam-based electrodes. The OER was investigated in 0.1 M NaOH solution at room temperature on as-received and Co- or Mo-modified Ni foam anodes. Corresponding values of charge-transfer resistance, exchange current-density for the OER and other electrochemical parameters for the examined Ni foam composites were recorded. The electrodeposition of Co or Mo on Ni foam base-materials resulted in a significant enhancement of the OER electrocatalytic activity. The quality and extent of Co, and Mo electrodeposition on Ni foam were characterized by means of scanning electron microscopy (SEM) and energy-dispersive X-ray spectroscopy (EDX) analysis.

1. Introduction

In recent years, the development of renewable energy sources has dramatically increased [1,2], resulting from both a gradual depletion of crude oil sources, as well as progressive degradation of the natural environment [3,4]. Unfortunately, currently-used green energy technologies are strongly dependent on weather conditions and topography. For instance, the energy production of solar panels reaches its peak value at noon; however, it does not meet the demands of energy consumption [5]. This phenomenon is well-known under the name of solar energy's duck curve. Appropriate storage of this energy excess could be the only solution to the above problem [6]. Currently, most of the produced renewable energy is stored in lithium-ion battery systems, because of their high-efficiency and convenience in exploitation. However, all batteries have their limitations, such as slow charge and discharge time, which is strongly dependent on ambient temperature, as well as limited operational lifetime. Moreover, used batteries could become environmentally important hazardous waste. One of the most promising new energy storage technologies is based on hydrogen generation by means of alkaline water electrolysis (AWE) [7,8]. Such produced hydrogen can be considered an entirely environmentally friendly energy carrier, since the only by-products generated during the hydrogen combustion are heat and water (see Equation (1)) [9].

$$2H_2 + O_2 \rightarrow 2H_2O + Q \tag{1}$$

While many catalysts are known to reduce the overpotential of hydrogen evolution reaction (HER), the more complex oxygen evolution (OER) process still requires a large

amount of energy to proceed. Contrary to a comparatively fast single-electron transfer cathodic process, the OER is related to a slow and complex, four-electron transfer reaction (see Equation (2)) [10,11].

$$4OH^- \rightarrow O_2 + 2H_2O + 4e^- \tag{2}$$

Hence, in order to minimize the overpotential of the OER, the researchers have made significant efforts in developing new types of anodes. As a result, electrodes based on ruthenium [12] and iridium [13] oxides were found to exhibit outstanding electrochemical properties towards the OER; however, because of their high costs, the use of these materials on the industrial scale is not economically practical. Therefore, in recent years, the researchers' attention has been shifted to more abundant and inexpensive transitional metals (Ni, Co, Mn, Mo, Fe) [14–16] and their alloys [17], oxides and carbides [18,19] to replace platinum group metals.

Thus, one of the most commonly used base materials to make electrodes, in the hydrogen production industry, are nickel and its derivatives. The employment of nickel and nickel-coated electrodes results from their unique properties, such as high catalytic activity in both hydrogen and oxygen evolution reactions. In addition, nickel exhibits superior anticorrosion properties in an alkaline environment. Generally, it is well-known that the OER on metals proceeds on the surface covered by their oxides, where nickel oxide/hydroxide species are especially catalytic in this reaction [20–26].

However, in order to compete with the electrocatalytic properties of electrodes based on noble metals, newly developed electrodes have to be characterized by large and highly active surface areas (HASA). Large values of HASA could be easily achieved by employing various materials, including foams, fibres, nanowires or nanocones. Such a base material could then be modified with a trace amount of transition metal(s) by one of the deposition methods (electrochemical, electroless, CVD: chemical vapour deposition or PVD: physical vapour deposition), which could further enhance the electrocatalytic properties of these innovative materials [20,21].

Nickel foam could be considered one of the most promising candidates for fabricating such a highly reactive anode in the process of the OER, as in addition to its unique electrocatalytic properties, Ni foam also provides large values of HASA. Nickel is also relatively inexpensive, compared to most noble metals [22].

In this work, electrochemically modified Ni foam materials were assessed as potential anodes towards the OER in alkaline 0.1 M NaOH environment through the employment of major electrochemical techniques. In addition, the structure and quality of electrodeposited Co and Mo on the surface of nickel foam were evaluated by means of a combined scanning electron microscopy (SEM) and energy-dispersive X-ray spectroscopy (EDX) methodology.

2. Results and Discussion

2.1. SEM/EDX Characterization of Ni Foam and Co-, and Mo-Modified Nickel Foam Electrodes

Figure 1a,b below illustrate SEM micrograph pictures of the electrodeposition effect of Co and Mo at small and trace amounts, respectively, on the Ni foam surface, recorded at the same magnification level. For the Co-modified Ni foam (at ca. 1 wt.% Co), the surface of the base material is densely covered with a granular structure of small Co nuclei (see Figure 1a). On the other hand, a sample of Mo-modified Ni foam (at ca. 0.2 wt.% Mo) is comparatively shown in a SEM micrograph picture of Figure 1b. The electrodeposited sample is covered with quite an irregular, amorphous and discontinuous structure through the Ni foam surface. In addition, the more detailed information on the composition of the prepared samples is shown in Table 1. Moreover, Figure 1c,d demonstrate the EDX pattern of Co- and Mo-modified Ni foam electrodes, respectively.

In addition, the SEM-approximated Co and Mo grain size value came to 50.0 ± 3.5 and 512 ± 9.8 nm, respectively. The above was performed through utilization of the Image Analysis Program (NIS-Elements Basic Research on Nikon).
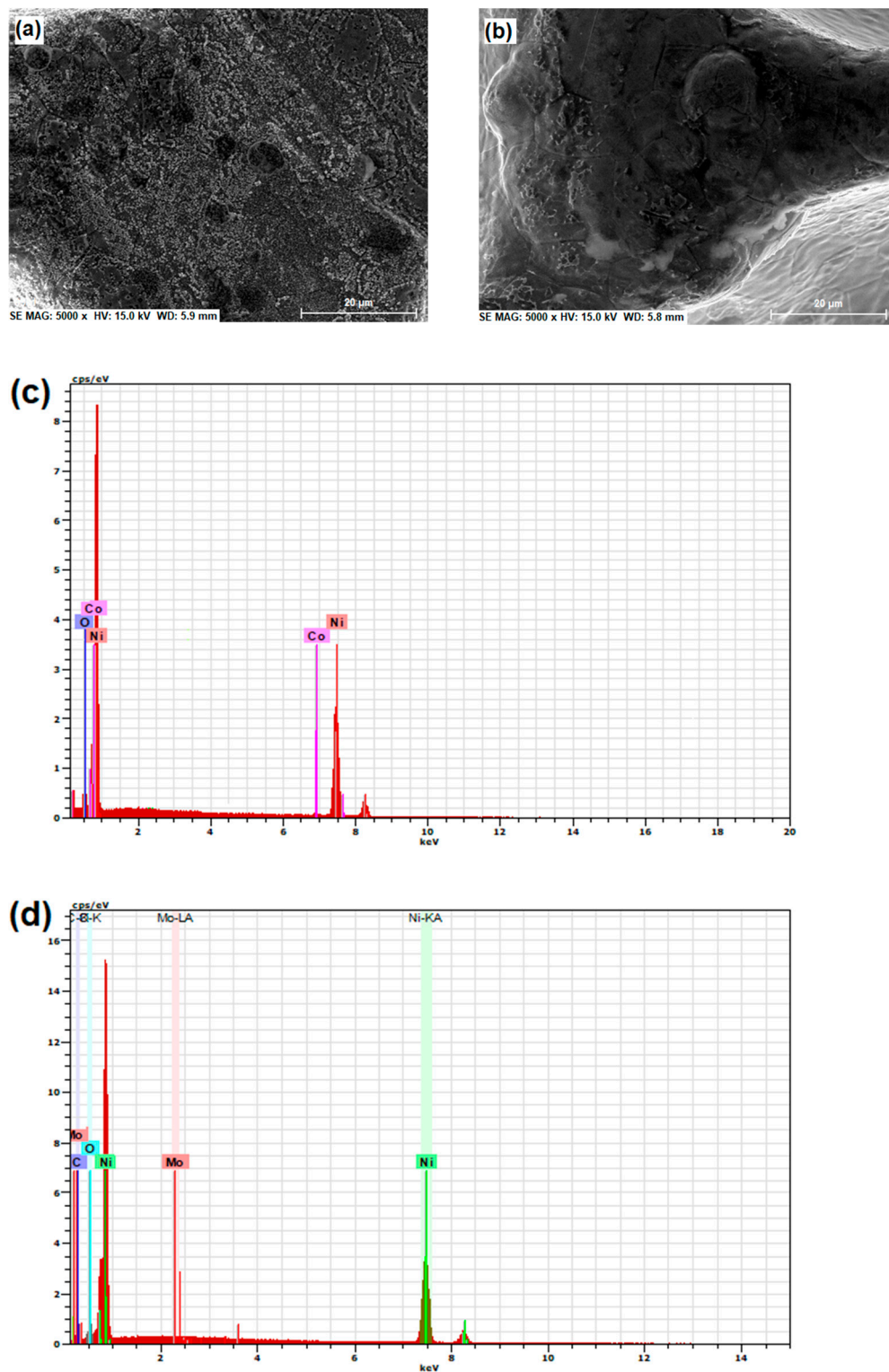
Figure 1. SEM micrograph pictures of Co-modified Ni foam surface (**a**), and Mo-activated Ni foam surface (**b**), taken at 5000× magnification with EDX pattern of Co- (**c**) and Mo-activated (**d**) Ni foam samples.

Table 1. EDX-derived (for an acceleration voltage of 15 kV) chemical composition of surface elements for freshly prepared: Co- and Mo-modified Ni foam samples.

	Element/%	Spectrum 1	Spectrum 2
Co-modified Ni foam	Ni	95.83	92.84
	Co	1.06	1.25
	O	3.11	5.91
	Total:	100.00	100.00
Mo-modified Ni foam	Ni	92.08	86.42
	Mo	0.25	0.33
	O	2.61	5.06
	C	5.06	8.19
	Total:	100.00	100.00

2.2. OER Characterizations of Ni Foam, Co- and Mo-Modified Ni Foam Electrodes

Cyclic voltammetry (CV) characterization of the surface oxidation process on fresh, Co- and Mo-modified Ni foam electrodes in 0.1 M NaOH solution during 50 CV sweeps, carried-out over the potential span 1.2–1.9 V/RHE (reversible hydrogen electrode) with a scan rate of 50 mV s^{-1} (only three last sweeps are presented) is shown in Figure 2 below. Thus, for pure and Co-modified nickel foam samples, the CV profiles displayed an oxidation peak (centred at ca. 1.49 and 1.45 V, correspondingly) along with a cathodic reduction peak (starting around 1.3 V). The Mo modification caused a shift of the oxidation peak to more positive potentials than that for pure Ni foam. In contrast, the reduction peak was no longer visible, as it was most likely moved outside the measured potential range. These features refer to the electrochemical formation of the surface β-NiOOH phase and its reduction to β-Ni(OH)$_2$ layer, correspondingly (Equation (3)).

$$\beta\text{-Ni(OH)}_2 + \text{OH}^- \leftrightarrow \beta\text{-NiOOH} + \text{H}_2\text{O} + \text{e}^- \tag{3}$$
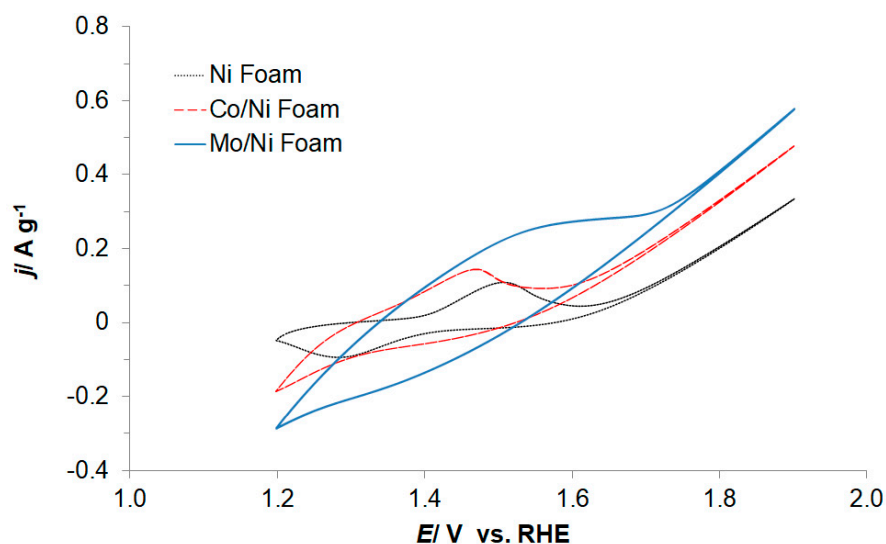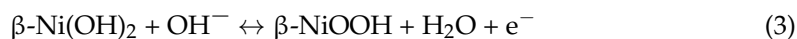
Figure 2. Cyclic voltammogram curves of oxidized, pure Ni, Co- and Mo-activated Ni foam electrodes, in contact with 0.1 M NaOH medium (at 20 °C), carried-out at a scan-rate of 50 mV s^{-1} for the potential span 1.2–1.9 V vs. RHE.

Tafel polarization plots recorded at room temperature for electrochemically oxidized, pure Ni foam, Mo- and Co-modified Ni foam electrodes are shown in Figure 3. Hence, for the nickel foam electrode, the recorded anodic Tafel slope (parameter b_a in Figure 3) and the Tafel-derived exchange current-density (j_0) value for the OER came to 54 mV dec^{-1} and 7.1×10^{-11} A cm^{-2} over the low overpotential range. The modification utilizing

surface Co or Mo deposition caused the values of b_a and j_0 parameters to rise to 83 and 74 mV dec^{-1}, and 7.0×10^{-8} and 9.6×10^{-8} A cm^{-2}, correspondingly, for the Co- and Mo-modified electrodes. Simultaneously, for larger overpotential values, the reaction system (not presented in Figure 3) moved into the mass transport limitations (see e.g., Ref. [27]). Pre-electrooxidation of Ni foam surfaces proved to be necessary to increase an initial value of the j_0 parameter for low overpotential range, as compared to an analogous Ni foam-based electrode by 3.6× [23]. Additionally, such-recorded exchange current-density was higher than that for other Ni foam [24] and similar 3D-structured [25] Ni electrodes by 7.0× and 1.6×, respectively. Moreover, as compared to similar catalysts [25], Mo-modified Ni foam electrode exhibited superior OER catalytic activity (with over 17× higher value of the j_0 parameter) to that of Ni-Mo composite coating.
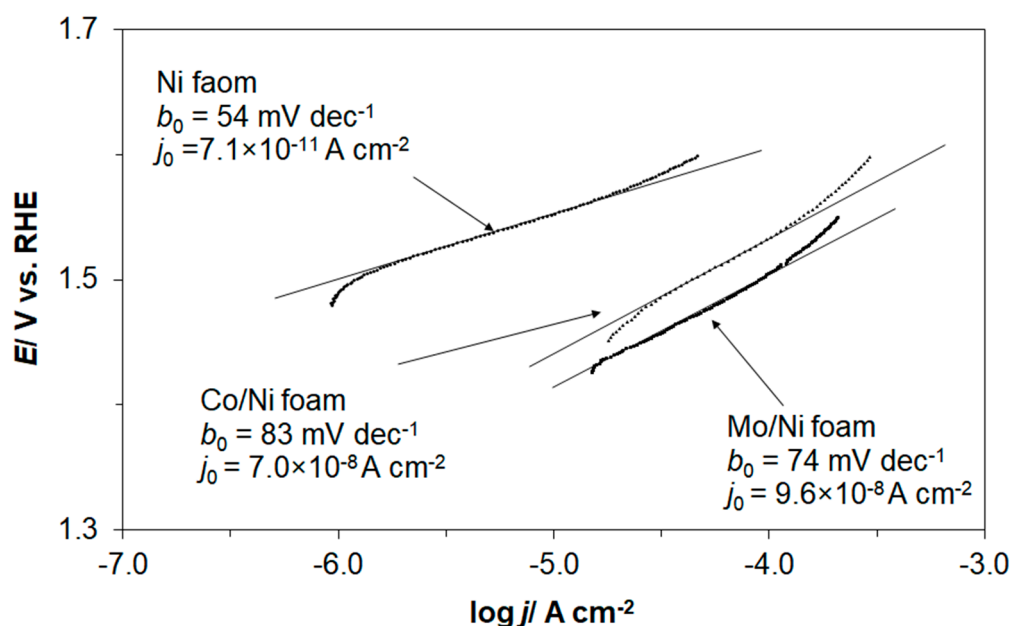

Figure 3. *Quasi*-potentiostatic anodic Tafel polarization curves (recorded at a scan-rate of 0.5 mV s^{-1}) for oxidized Ni foam, Co- and Mo-activated Ni foam electrodes, carried out in 0.1 M NaOH solution (appropriate iR corrections were made based on the solution resistance derived from impedance measurements); calculated Tafel slopes for oxidized Ni foam, Co- and Mo-modified Ni foam samples came to b_a = 54, 83 and 74 mV dec^{-1}, correspondingly.

Nowadays, there is a trend in literature to show the Tafel polarization results for a set overpotential, typically at η = 0.300 V or a set current-density, usually at 10 mA cm^{-2} [26,27]. Hence, the current densities at η = 0.3 V for the Co-modified Ni foam electrode came to 9.2×10^{-5} A cm^{-2}, which was superior to those recorded in literature for various cobalt-modified anodes (see e.g., the recorded values of 1.4×10^{-6}–1.0×10^{-5} A cm^{-2} for cobalt oxide electrodes by Lyons and Brandon in Ref. [28]. On the other hand, the recorded b_a parameter for the examined electrodes was similar to those derived on Co and Mo modified 3D-structured electrodes (39 to 80 mV dec^{-1}) by Kubisztal and Budniok, Badruzzaman et al. and Lyons, and Brandon in References [25–27].

In order to further characterize the electrocatalytic properties of Ni foam-based electrodes towards the OER, the electrochemical impedance spectroscopy (EIS) technique was applied. The complex-plane EIS spectra are shown in Figure 4. It should be mentioned that all electrodes have exhibited two somewhat depressed semicircles, where the high-frequency arc could be associated with the kinetics of the oxygen evolution reaction (interfacial charge-transfer reaction step). In contrast, the intermediate/low-frequency semicircle corresponds to the surface adsorption of the reaction intermediates [29–34]. The electrochemical parameters [Faradic reaction resistance (R_{ct}), the adsorption resistance

for reaction intermediates (R_{Ads}), double-layer capacitance (C_{dl}) and pseudo-capacitance (C_{Ads})] were obtained by means of two constant phase element (CPE)-modified Randles equivalent circuit model (Figure 5), and their values are presented in Table 2. The CPE element was used within the circuit in order to account for the capacitance dispersion effect, represented by distorted semicircles in the Nyquist impedance plots.
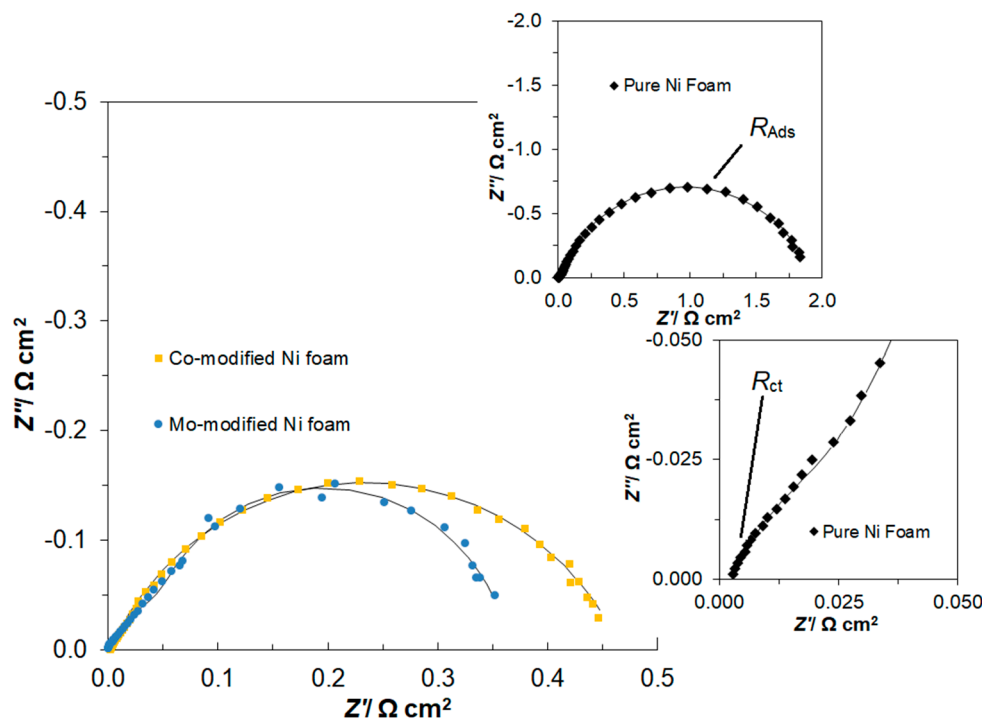

Figure 4. Electrochemical impedance Nyquist plots for the OER on oxidized Ni foam, Co- and Mo-modified Ni foam electrode surfaces in contact with 0.1 M NaOH (at 20 °C) for the potential of 1.6 V vs. RHE. The solid line corresponds to representation of the data according to equivalent circuit presented in Figure 5 below.
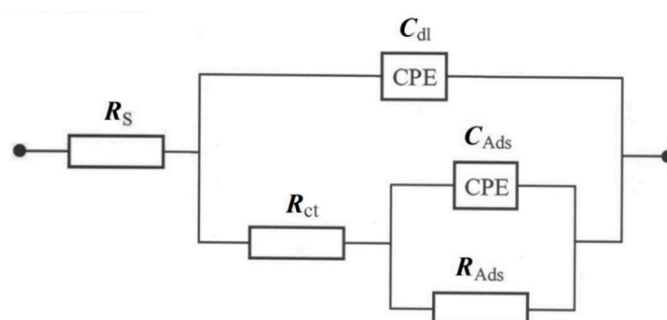

Figure 5. Equivalent circuit for impedance analysis of the OER process. Two CPE-R element equivalent circuit was used for fitting the impedance data for as received Ni foam, Co- and Mo-activated Ni foam electrodes, obtained in 0.1 M NaOH solution. The circuit includes two constant phase elements (CPEs), to account for distributed capacitance; R_{ct}, C_{dl}, R_{Ads}, and C_{Ads} (as CPE) elements correspond to the charge-transfer resistance, interfacial double-layer capacitance, resistance and capacitance adsorption components of reaction intermediates; R_{s} is solution resistance.

Thus, for the oxidized Ni foam electrode, the recorded R_{ct} parameter diminished from 0.187 Ω g to 0.047 Ω g at η = 270 and 620 mV, respectively. Similarly, the C_{dl} parameter decreased from the value of 120,933 to reach 8720 μF g^{-1} s$^{\varphi 1-1}$ for the same overpotential span (see Table 2 for details). The above effect could be associated with substantial blocking of the electrode surface by freshly formed O$_2$ bubbles, which could easily be visually

noticed, especially at increased anodic overpotentials. Simultaneously, the value of the R_{Ads} parameter reduced from 41.756 to 0.123 Ω g for the corresponding potential range, while the C_{Ads} parameter oscillated between an initial value of 144,293 (at 270 mV) and a minimum value of 67,867 μF g^{-1} s$^{\varphi 2 -1}$ recorded at 420 mV. The latter understandably implies that the kinetics of the OER become facilitated upon the rise of the dc electrode potential. However, the R_{Ads} parameter values shown in Table 2 are essentially larger than those recorded for the R_{ct} parameter. The above suggests that the OER process is limited by the reaction intermediates' adsorption kinetics (also see References [23,34]).

Table 2. Electrochemical parameters for the OER, obtained at as received Ni foam, Co- and Mo-modified Ni foam electrodes in contact with 0.1 M NaOH supporting solution. The results obtained here were recorded by fitting the CPE-modified Randles equivalent circuit (see Figure 5) to the experimentally obtained impedance data (reproducibility usually below 10%, $\chi^2 = 4.03 \times 10^{-5}$ to 1.07×10^{-3}.

η/mV	R_{ct}/Ω g	C_{dl}/μF g^{-1} s $^{\varphi 1 -1}$	R_{Ads}/Ω g	C_{Ads}/μF g^{-1} s $^{\varphi 2-1}$
		Ni Foam		
270	0.187 ± 0.033	120,933 ± 12,554	41.756 ± 4.524	144,293 ± 11,985
320	0.129 ± 0.025	127,147 ± 12,430	9.047 ± 0.206	103,520 ± 11,383
370	0.073 ± 0.008	114,453 ± 6488	1.844 ± 0.105	81,360 ± 5257
420	0.086 ± 0.008	89,627 ± 3612	0.616 ± 0.008	67,867 ± 2587
470	0.075 ± 0.007	81,493 ± 3352	0.289 ± 0.007	73,840 ± 3282
520	0.061 ± 0.005	67,600 ± 3119	0.176 ± 0.005	90,933 ± 3627
570	0.064 ± 0.005	76,773 ± 2646	0.114 ± 0.005	78,717 ± 5113
620	0.047 ± 0.002	8720 ± 414	0.123 ± 0.003	129,227 ± 9950
		Co-modified Ni foam		
270	0.052 ± 0.006	541,047 ± 15,371	5.265 ± 0.417	670,980 ± 28,526
320	0.035 ± 0.004	224,899 ± 26,583	1.239 ± 0.009	690,541 ± 6229
370	0.030 ± 0.004	218,716 ± 10,076	0.217 ± 0.004	412,736 ± 7235
420	0.027 ± 0.003	188,682 ± 8730	0.214 ± 0.004	444,831 ± 6886
470	0.028 ± 0.003	141,993 ± 5113	0.128 ± 0.003	475,169 ± 10,406
520	0.024 ± 0.002	121,588 ± 3725	0.089 ± 0.002	488,446 ± 13,374
570	0.024 ± 0.002	161,622 ± 5287	0.052 ± 0.002	576,419 ± 31,772
620	0.022 ± 0.004	105,473 ± 9599	0.041 ± 0.005	557,230 ± 91,804
		Mo-modified Ni foam		
270	0.081 ± 0.011	822,987 ± 85,015	2.274 ± 0.052	1,743,525 ± 143,562
320	0.069 ± 0.010	540,724 ± 66,936	0.667 ± 0.018	1,916,698 ± 61,430
370	0.066 ± 0.009	599,202 ± 157,063	0.296 ± 0.007	1,680,668 ± 168,453
420	0.068 ± 0.017	1,024,082 ± 152,342	0.181 ± 0.014	1,045,659 ± 157,476
470	0.052 ± 0.004	200,204 ± 20,927	0.150 ± 0.006	1,512,226 ± 94,060
520	0.035 ± 0.008	783,766 ± 74,144	0.111 ± 0.008	1,337,607 ± 118,659
570	0.030 ± 0.011	1,008,571 ± 140,070	0.091 ± 0.011	916,327 ± 126,682
620	0.023 ± 0.003	1,271,429 ± 181,585	0.087 ± 0.003	1,524,620 ± 324,842

Then, the R_{ct} parameter for the Co and Mo-modified Ni foam electrodes ranged from 0.052 to 0.022 Ω g and from 0.081 to 0.023 Ω g for the overpotential range: 270–620 mV, respectively. The former implies a considerable reduction of the R_{ct} parameter (as compared to those R_{ct} values recorded for the oxidized Ni foam surface); namely, by 3.6× and 2.3× at 270 mV, and by 2.1× at 620 mV for the Co and Mo-modified catalyst materials, respectively (see again Table 2 for details). Similarly, changing radius of the low-frequency semicircle (adsorption of reaction intermediates response) also resulted in a relatively constant decrease of the R_{Ads} parameter value by ca. 8× and 3× for the cobalt-based, and by 18× and 1.4× for the Mo-modified Ni foam electrodes for the overpotentials of 270 and 620 mV.

Furthermore, deposition of catalytic nanostructures (see Figure 1a,b) resulted in a considerable enhancement of the electrochemically accessible surface area. The latter could be easily observed in the cyclic voltammetry plot presented for the baseline and

the Co and Mo-modified Ni foam materials in Figure 2. Consequently, significant surface modification for the Co- and Mo-modified Ni foams is demonstrated by considerably increased current-density within the corresponding CV profiles.

The reported values of the C_{dl} parameter at η = 270 mV came to 541,047 $\mu F\ g^{-1}\ s\ ^{\varphi 1-1}$ (Co-modified Ni foam) and 822,987 $\mu F\ g^{-1}\ s\ ^{\varphi 1-1}$ for the Mo-based Ni foam catalyst material, which translates to ca. 4.5× and 6.8× augmentation of the HASA values for both modified electrodes, in contrast to the oxidized Ni foam anode. Once these surface coefficients are referred to the previously calculated ratios of the R_{ct} parameter, it becomes evident that the cobalt-activated nickel foam anode exhibited superior OER performance. In addition, dimensionless φ_1 and φ_2 parameters (where φ determines the constant phase angle in the complex-plane plot and $0 \leq \varphi \leq 1$) of the CPE circuits (see Figure 5) oscillated between: 0.66–0.97 and 0.49–0.97, respectively.

The impedance results obtained for the examined electrodes in this work were generally in line with those OER impedance studies presented by Si et al. [35] and by Lyons, and Brandon [28] on cobalt oxide electrodes, and by Choi et al. [36] and by Wu, and He [37] on Mo-based composites. Moreover, Table 3 presents a comparison of the impedance-recorded R_{ct} and j (polarization plot-estimated for η = 0.3 V) parameter values in this work (the charge-transfer resistance was derived through the C_{dl}-approximated surface area of the nickel foam electrodes [23,38,39]) with the results recorded on similar electrodes in References [35–37]. It should be noted that the R_{ct} results presented for Ni-Mo based electrodes in Refs. [36,37] were given as raw data, without providing any specific information on the electrodes' surface area. Thus, in order to make a meaningful comparison, one could estimate the HASA values through dividing the recorded interfacial capacitance by a commonly used value of 20 mF cm^{-2} in literature for smooth and homogeneous surfaces (see Refs. [38,39]). Having done so, the surface-normalized R_{ct} parameter would come to 981 and 364 Ω cm^2 for Ni-Fe-C-Mo and NiMoO$_4$ electrode surfaces, correspondingly. These estimated resistance values are radically greater than those recorded in this work. In addition, the plot-derived value of the j parameter (1.15×10^{-5} A cm^{-2}) for Co oxide/Fe electrode came very close to the current-densities recorded in this work.

Table 3. Electrochemical parameters for the OER performed at the surfaces of different catalyst materials, under alkaline conditions.

η/mV	Solution	Catalysts	R_{ct}/Ω cm^2	$j_{(\eta = 0.3V)}$/A cm^{-2}	Ref.
270	0.1 M NaOH	Co-modified Ni foam	31.9	9.2×10^{-5}	This work
420	0.1 M NaOH	Co-modified Ni foam	16.6	-	This work
430	0.1 M KOH	Co(OH)$_2$/C	8.5	-	35
420	0.1 M NaOH	Co oxide/Fe	17.5	1.15×10^{-5}	28
270	0.1 M NaOH	Mo-modified Ni foam	27.1	1.6×10^{-4}	This work
420	0.1 M NaOH	Mo-modified Ni foam	22.6	-	This work
290	1.0 M KOH	NiMoO$_4$ nanowire/Ni foam	981 *	-	36
210	30% KOH	Ni-Fe-C-Mo/Ni mesh	364 *	-	37
438	1.0 M NaOH	Pt	80	~4×10^{-5} **	40
278	0.1 M KOH	RuO$_2$/GC ***	142 *	~5×10^{-4} **	41
250	0.1 M KOH	Pd/FTO ****	42 *	~12×10^{-3} **	42

* surface-normalized values (see information below); ** values estimated from the Tafel plots; *** glassy carbon; **** fluorine-doped tin oxide.

Furthermore, in order to fully access the suitability (and possibly also superiority) of the developed electrodes for their possible commercial use, Table 3 also presents the R_{ct} and j (η = 0.3 V) parameter values for the OER, obtained on selected noble metals/oxide (Pt, RuO$_2$ and Pd), under similar experimental conditions [40–42]. Hence, the recorded (or estimated) charge-transfer resistance parameter values for bulk Pt, RuO$_2$/GC and Pd/FTO electrodes were significantly greater than those recorded for the Co (or Mo)-modified nickel foam specimens. On the other hand, only fluorine-doped tin oxide palladium

electrode exhibited radically higher values (ca. 12×10^{-3} A cm^{-2}) of Tafel plot-derived current-density parameter than those recorded in the present work for the catalyst (Co, Mo)-modified nickel foam materials.

In addition, the exchange current-density values (j_0) for the OER recorded for Co- and Mo-modified Ni foam samples were calculated based on the linear dependence of -log R_{ct} vs. overpotential/η, fulfilled by kinetically controlled reactions through employing the Butler-Volmer equation and the relation between the j_0 and the R_{ct} parameter for overpotential approaching 0 [43,44]. Hence, the impedance-based exchange current-density value for the studied overpotential range (η = 270–620 mV with 50 mV potential increments) came to 6.06×10^{-5} A cm^{-2} for the as-received Ni foam sample. However, significantly higher values of the j_0 parameter were recorded for both Co- and the Mo-modified Ni foam samples, i.e., 2.89×10^{-4} A cm^{-2} and 1.04×10^{-4} A cm^{-2}, correspondingly (see Figure 6 below). In addition, the R_{ct}-derived exchange-current densities are somewhat higher in comparison to those of other OER works performed on electrodes modified by Co and Mo elements in alkaline solutions [25,45]. There, the exchange current-density values recorded for Ni + Mo composite coating came to 9.7×10^{-5} A cm^{-2} [25] and 5.2×10^{-5} A cm^{-2} [45]. Similarly, values of the j_0 parameter, recorded for high overpotential range on Co-based compsite electrodes came to 3.5×10^{-5} A cm^{-2} [46] and 1.1×10^{-5} A cm^{-2} [28].
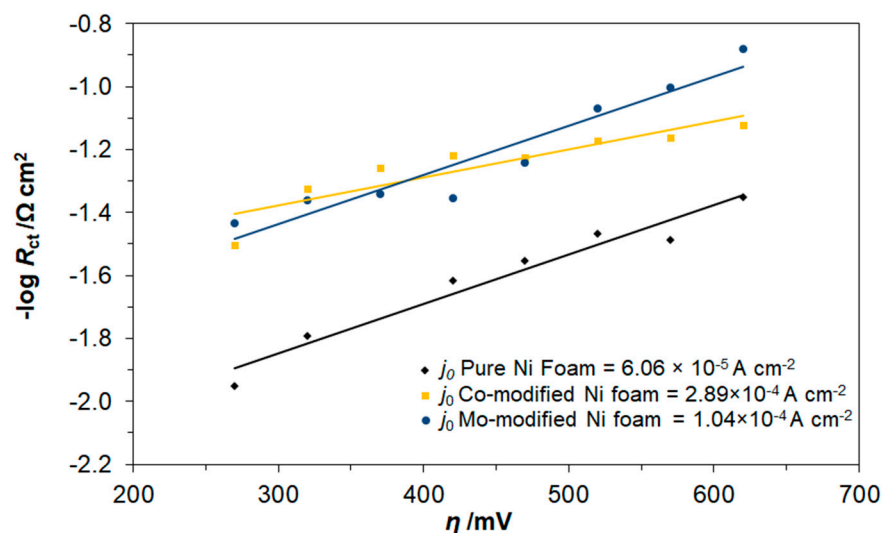

Figure 6. −log R_{ct} vs. overpotential relationship for the OER on oxidized pure Ni foam, Co- and Mo-activated Ni foam electrode surfaces, carried-out in 0.1 M NaOH solution.

3. Materials and Methods

3.1. Solutions and Chemical Reagents

In this work, all supporting solutions were prepared by dissolving chemical reagents in ultra-pure water (18.2 MΩ cm) from the Hydrolab (Spring 30 s) purification system. 0.1 M NaOH working electrolyte was prepared from sodium hydroxide pellets (99.996%, AESAR, Ward Hill, NY, USA). Before each series of experiments, atmospheric air was removed from central and both side cell's compartments by bubbling with high purity argon (Ar 6.0 grade, Linde, Puławy, Poland) for 15 and 5 min, respectively. Furthermore, argon gas flow was kept above the solutions throughout the experiments. 0.5 M H$_2$SO$_4$ (stock H$_2$SO$_4$: 96%, Merck, Darmstadt, Germany) solution was used for periodic charging of a Pd reversible hydrogen electrode (RHE).

3.2. Preparation of Electrochemical Cell and Electrodes

The OER activity of pure Ni foam, Co- and Mo-modified Ni foam electrodes was examined in an electrochemical cell made of Pyrex glass. The cell comprised three separate compartments. In the central compartment, a Ni foam-based working electrode (WE) was

placed, when both Pd (1.0 mm diameter wire, 99.98+% purity, AlfaAesar, Ward Hill, NY, USA) reversible hydrogen electrode and a Pt (1.0 mm diameter wire, 99.9998% purity, Johnson Matthey, Inc., London, UK) counter electrode (CE) were located in separate side compartments.

Nickel foam base electrode material was delivered by MTI Corporation (Richmond, CA, USA) (purity: >99.99% Ni; thickness: 1.6 mm; surface density: 346 g m^{-2}; porosity: $\geq$95%; estimated electrochemically active surface 14.9 cm^2) [38]. All examined electrodes were 1 cm $\times$ 1 cm (ca. 35 mg). Before electrodeposition of Co and Mo elements on Ni foam base material, freshly cut foam samples were degreased in acetone bath for 15 min under ultrasonication. Then, they were air dried and etched in 2 M HCl for 15 min at 60 °C, also under ultrasonication. Electrodeposition of Co and Mo catalysts on Ni foam was performed according to the conditions and bath compositions shown in Table 4. The bath's pH for Co electrodeposition was readjusted with 0.1 M NaOH or 0.1 M HCl solutions prior to the experiment. Similarly, before electrodeposition of Mo, the solution's pH was modified with 0.1 M NaOH, accordingly. No significant pH change was observed during both metal deposition trials.

Table 4. Operating parameters and bath compositions employed for electrodeposition of Co and Mo onto Ni foam substrate.

Bath Constituents	Concentration (M)	Operating Parameters
Electrodeposition of Co		
CoCl$_2$ $\times$ 6 H$_2$O (99%, Sigma Aldrich, Saint Louis, MO, USA)	0.10	Anode: Pt foil
NaCl (99.9%, POCH, Gliwice, Poland)	0.02	Cathode: Ni foam Temperature: 303 K Deposition time: 300 s Current-density: 0.52 mA cm^{-2} Solution pH: 4.5
Electrodeposition of Mo		
(NH$_4$)$_6$Mo$_7$O$_{24}$·4H$_2$O ($\geq$99.3%, Merck, Darmstadt, Germany) CH$_3$CO$_2$NH$_4$ ($\geq$98.0%, Merck, Darmstadt, Germany) CH$_3$COOK ($\geq$99.0%, Sigma Aldrich, Saint Louis, USA)	1.95 $\times$ 10^{-4} 0.26 0.26	Anode: Pt foil Cathode: Ni foam Temperature: 303 K Deposition time: 1800 s Current density: 5.2 mA cm^{-2} Solution pH: 6.8

Such-modified Ni foam materials were left in a desiccator for an extended period of time before being weighed. Before conducting a series of electrochemical experiments, as received, Co- and Mo-modified Ni foam samples underwent extensive electrooxidation by means of 50 cyclic voltammetry sweeps, carried-out for the potential range 1.2–1.9 V/RHE, at a sweep rate of 50 mV s^{-1}.

The palladium RHE was sealed in soft glass. Before its use, the reference electrode was cleaned in hot, concentrated sulphuric acid, followed by cathodic (galvanostatic) charging with hydrogen in 0.5 M H$_2$SO$_4$ until H$_2$ bubbles in the electrolyte were clearly visible. The stability of such prepared RHE was occasionally checked by recording its potential shift in time (it should then be noted that all potentials throughout this work are given on the RHE scale). The CE electrode, prior to its use, was flame-annealed. Similarly, before each series of electrochemical experiments, the electrochemical cell was taken apart and soaked in hot sulphuric acid for at least 4 h. After having been cooled to about 30 °C, the cell was thoroughly rinsed with Hydrolab ultra-pure water.

3.3. Experimental Methodology

Electrochemical performance of the OER electrocatalysts (pure Ni foam, Co-, and Mo-modified Ni foam electrodes) was conducted by a.c. impedance spectroscopy and quasi steady-state Tafel polarization techniques by means of an AUTM204 + FRA32M

Multi-Autolab potentiostat/galvanostat system, at room temperature (293 K). For the a.c. impedance measurements, the generator provided an output signal of 5 mV rms and the frequency was swept between 1.0×10^5 and 2×10^{-2} Hz. The instruments were controlled by *Nova 2.1* software for Windows (Metrohm Autolab B.V., Opacz-Kolonia, Poland). Also, all data analysis was performed with the above-mentioned software package. Typically, three impedance measurements were performed at each potential value, independently at two foam electrodes, where reproducibility of such obtained results was usually below 10%. The obtained impedance spectra were fitted by means of a complex, nonlinear, least-squares immittance fitting program. Furthermore, quasi-potentiostatic anodic polarization experiments (recorded at a scan-rate of 0.5 mV s^{-1}) for the OER were carried-out at all Ni foam-based samples.

Additionally, SEM/EDX surface spectroscopy characterization of all examined (Ni foam, Co- and Mo-modified Ni foam) samples was carried out by means of Merlin FE-SEM microscope (Zeiss, Jena, Germany), equipped with Bruker XFlash 5010 EDX instrumentation (with 125 eV resolution) (Bruker, Billerica, MA, USA).

4. Conclusions

Electrochemically deposited small amounts of transition metals in the form of cobalt (at ~1 wt.%) and molybdenum (at ~0.28 wt.%) nanoparticle deposits on the surface of Ni foam material significantly enhanced catalytic activity of the base foam material towards anodic evolution of oxygen in 0.1 M NaOH solution. The above is primarily related to superior OER catalytic properties of Co and Mo nano-deposits, in addition to the considerable modification of electrochemically-active surface for these catalyst materials. The results of this work showed a real possibility for replacing expensive and scarcely found in the natural environment noble metals with significantly cheaper transition metals for the mass production of commercial alkaline water electrolysers.

Author Contributions: Conceptualization, B.P.; methodology, B.P., M.Ł. and T.M.; investigation, M.Ł., M.K; data curation, T.M., M.L. and M.K.; writing—original draft preparation, M.Ł., T.M.; editing, B.P. and T.M.; supervision, I.M.K. All authors have read and agreed to the published version of the manuscript.

Conflicts of Interest: The authors declare no conflict of interest.

References

1. Martins, F.; Felgueiras, C.; Smitkova, M.; Caetano, N. Analysis of Fossil Fuel Energy Consumption and Environmental Impacts in European Countries. *Energies* **2019**, *12*, 964. [CrossRef]
2. Krane, J. Climate change and fossil fuel: An examination of risks for the energy industry and producer states. *MRS Energy Sustain.* **2017**, *4*, 1–12. [CrossRef]
3. Dorning, M.A.; Diffendorfer, J.E.; Loss, S.R.; Bagstad, K.J. Review of indicators for comparing environmental effects across energy sources. *Environ. Res. Lett.* **2019**, *14*, 103002. [CrossRef]
4. Solarin, S.A. An environmental impact assessment of fossil fuel subsidies in emerging and developing economies. *Environ. Impact Assess. Rev.* **2020**, *85*, 106443. [CrossRef]
5. Kåberger, T. Progress of renewable electricity replacing fossil fuels. *Glob. Energy Interconnect.* **2018**, *1*, 48–52.
6. Wang, Q.; Chang, P.; Bai, R.; Liu, W.; Dai, J.; Tang, Y. Mitigation Strategy for Duck Curve in High Photovoltaic Penetration Power System Using Concentrating Solar Power Station. *Energies* **2019**, *12*, 3521. [CrossRef]

7. Züttel, B.A.; Remhof, A.; Borgschulte, A.; Friedrichs, O. Hydrogen: The future energy carrier. *Philos. Trans. R. Soc. Lond. Ser. A* **2010**, *358*, 3329–3342. [CrossRef] [PubMed]

8. Khan, M.A.; Al-Shankiti, L.; Ziani, A.; Idriss, H. Demonstration of green hydrogen production using solar energy a 28% efficiency and evaluationof its economic viability. *Sustain. Energy Fuels* **2021**, *5*, 1085–1094. [CrossRef]

9. Dincer, I. Green methods for hydrogen production. *Int. J. Hydrogen Energy* **2012**, *37*, 1954–1971. [CrossRef]

10. Tahira, M.; Pana, L.; Idreesd, F.; Zhanga, X.; Wanga, L.; Zoua, J.J.; Wang, Z.L. Electrocatalytic oxygen evolution reaction for energy conversion and storage: A comprehensive review. *Nano Energy* **2017**, *37*, 136–157. [CrossRef]

11. Divanis, S.; Kutlusoy, T.; Boye, I.M.I.; Man, I.C.; Rossmeisl, J. Oxygen evolution reaction: A perspective on a decade of atomic scale simulations. *Chem. Sci.* **2020**, *11*, 2943–2950. [CrossRef]

12. Kuo, D.-Y.; Paik, H.; Kloppenburg, J.; Faeth, B.; Shen, K.M.; Schlom, D.G.; Hautier, G.; Suntivich, J. Measurements of Oxygen Electroadsorption Energies and Oxygen Evolution Reaction on RuO_2(110): A Discussion of the Sabatier Principle and Its Role in Electrocatalysis. *J. Am. Chem. Soc.* **2018**, *140*, 17597–17605. [CrossRef] [PubMed]

13. Pérez-Viramontes, N.J.; Collins-Martínez, V.H.; Escalante-García, I.L.; Flores-Hernández, J.R.; Galván-Valencia, M.; Durón-Torres, S.M. Ir-Sn-Sb-O Electrocatalyst for Oxygen Evolution Reaction: Physicochemical Characterization and Performance in Water Electrolysis Single Cell with Solid Polymer Electrolyte. *Catalysts* **2020**, *10*, 524. [CrossRef]

14. Sanchez, J.; Ramos-Garcés, M.V.; Narkeviciute, I.; Colón, J.L.; Jaramillo, T.F. Transition Metal-Modified Zirconium Phosphate Electrocatalysts for the Oxygen Evolution Reaction. *Catalysts* **2017**, *7*, 132. [CrossRef]

15. Yuan, N.; Jiang, Q.; Li, J.; Tang, J. A review on non-noble metal based electrocatalysis for the oxygen evolution reaction. *Arab. J. Chem.* **2020**, *13*, 4294–4309. [CrossRef]

16. Dou, Y.; He, C.-T.; Zhang, L.; Al-Mamun, M.; Guo, H.; Zhang, W.; Xia, Q.; Xu, J.; Jiang, L.; Wang, Y.; et al. How Cobalt and Iron Doping Determine The Oxygen Exolution Electrocatalytic Activity of NiOOH. *Cell Rep. Phys. Sci.* **2020**, *1*, 1–14.

17. Milikić, J.; Balčiūnaitė, A.; Sukackienė, Z.; Mladenović, D.; Santos, D.M.F.; Tamašauskaitė-Tamašiūnaitė, L.; Šljukić, B. Bimetallic Co-Based (CoM, M = Mo, Fe, Mn) Coatings for High-Efficiency Water Splitting. *Materials* **2021**, *14*, 92. [CrossRef]

18. Kim, J.; Lee, D.H.; Yang, Y.; Chen, K.; Liu, C.; Kang, J.; Li, O.L. Hybrid Molybdenum Carbide/Heteroatom-Doped Carbon Electrocatalyst for Advanced Oxygen Evolution Reaction in Hydrogen Production. *Catalysts* **2020**, *10*, 1290. [CrossRef]

19. Wang, Y.; Wu, Q.; Zhang, B.; Tian, L.; Li, K.; Zhang, X. Recent Advances in Transition Metal Carbide Electrocatalysts for Oxygen Evolution Reaction. *Catalysts* **2020**, *10*, 1164. [CrossRef]

20. Ishaque, M.; Shah, A.; Iftikhar, F.J.; Akbar, M. Development of transition metal based electrolyzer for efficient oxygen evolution reaction. *J. Renew. Sustain. Energy* **2020**, *12*, 024102. [CrossRef]

21. Mikołajczyk, T.; Slis, A.; Solodovnik, T. Electrochemical Study of the Oxygen Evolution Reaction on MoNi/Carbon Fibre Electrode in 0.1 M NaOH. *Int. J. Electrochem. Sci.* **2019**, *14*, 1773–1781. [CrossRef]

22. Chaudhari, N.K.; Jin, H.; Kim, B.; Lee, K. Nanostructured materials on 3D nickel foam as electrocatalysts for water splitting. *Nanoscale* **2017**, *9*, 12231–12247. [CrossRef] [PubMed]

23. Pierozynski, B.; Mikolajczyk, T.; Luba, M.; Zolfaghari, A. Kinetics of oxygen evolution reaction on nickel foam and platinum-modified nickel foam materials in alkaline solution. *J. Electroanal. Chem.* **2019**, *847*, 113194. [CrossRef]

24. Van Drunen, J.; Pilapil, B.K.; Makonnen, Y.; Beauchemin, D.; Gates, B.D.; Jerkiewicz, G. Electrochemically Active Nickel Foams as Support Materials for Nanoscopic Platinum Electrocatalysts. *ACS Appl. Mater. Interfaces* **2014**, *6*, 12046–12061. [CrossRef]

25. Kubisztal, J.; Budniok, A. Study of the oxygen evolution reaction on nickel-based composite coatings in alkaline media. *Int. J. Hydrogen Energy* **2008**, *33*, 4488–4494. [CrossRef]

26. Badruzzaman, A.; Yuda, A.; Ashok, A.; Kumar, A. Recent advances in cobalt based heterogeneous catalysts for oxygen evolution reaction. *Inorg. Chim. Acta* **2020**, *511*, 119854. [CrossRef]

27. Lyons, M.E.; Brandon, M.P. A comparative study of the oxygen evolution reaction on oxidized nickel, cobalt and iron electrodes in base. *J. Electroanal. Chem.* **2010**, *641*, 119–130. [CrossRef]

28. Lyons, M.E.G.; Brandon, M.P. The Oxygen Evolution Reaction on Passive Oxide Covered Transition Metal Electrodes in Alkaline Solution. Part III—Iron. *Int. J. Electrochem. Sci.* **2008**, *3*, 1463–1503.

29. Doyle, R.L.; Lyons, M.E.G. An electrochemical impedance study of the oxygen evolution reaction at hydrous iron oxide in base. *Phys. Chem. Chem. Phys.* **2013**, *15*, 5224–5237. [CrossRef] [PubMed]

30. Lyons, M.E.G.; Brandon, M.P. The oxygen evolution reaction on passive oxide covered transition metal electrodes in aqueous alkaline solution. Part 1-nickel. *Int. J. Electrochem. Sci.* **2008**, *3*, 1386–1424.

31. Han, G.-Q.; Liu, Y.-R.; Hu, W.-H.; Dong, B.; Li, X.; Shang, X.; Chai, Y.-M.; Liu, Y.-Q.; Liu, C.-G. Three dimensional nickel oxides/nickel structure by in situ electro-oxidation of nickel foam as robust electrocatalyst for oxygen evolution reaction. *Appl. Surf. Sci.* **2015**, *359*, 172–176. [CrossRef]

32. Lyons, M.E.; Brandon, M.P. The significance of electrochemical impedance spectra recorded during active oxygen evolution for oxide covered Ni, Co and Fe electrodes in alkaline solution. *J. Electroanal. Chem.* **2009**, *631*, 62–70. [CrossRef]

33. Costa, F.R.; Franco, D.V.; Da Silva, L.M. Electorchemical impedance spectroscopy study of the oxygen evolution reaction on a gas-evolving anode composed of lead dioxide microfibers. *Electrochim. Acta* **2013**, *90*, 332–343. [CrossRef]

34. Franco, D.V.; Da Silva, L.M.; Jardim, W.F.; Boodts, J.F.C. Influence of the electrolyte composition on the kinetics of the oxygen evolution reaction and ozone production processes. *J. Braz. Chem. Soc.* **2006**, *17*, 746–757. [CrossRef]

35. Si, Y.; Guo, C.; Xie, C.; Xiong, Z. An Ultrasonication-Assisted Cobalt Hydroxide Composite with Enhanced Electrocatalytic Activity toward Oxygen Evolution Reaction. *Materials* **2018**, *11*, 1912. [CrossRef] [PubMed]

36. Choi, J.; Kim, D.; Zheng, W.; Yan, B.; Li, Y.; Yong, L.; Lee, L.Y.S.; Piao, Y. Interface engineered $NiFe_2O_{4-x}/NiMoO_4$ nanowire arrays for electrochemical oxygen evolution. *Appl. Catal. B Environ.* **2021**, *286*, 119857. [CrossRef]

37. Wu, Y.; He, H. Electrodeposited nickel–iron–carbon–molybdenum film as efficient bifunctional electrocatalyst for overall water splitting in alkaline solution. *Int. J. Hydrogen Energy* **2019**, *44*, 1336–1344. [CrossRef]

38. Pierozynski, B.; Mikolajczyk, T.; Kowalski, I.M. Hydrogen evolution at catalytically-modified nickel foam in alkaline solution. *J. Power Sources* **2014**, *271*, 231–238. [CrossRef]

39. Pierozynski, B.; Mikolajczyk, T. On the Temperature Dependence of Hydrogen Evolution Reaction at Nickel Foam and Pd-Modified Nickel Foam Catalysts. *Electrocatalysis* **2015**, *6*, 51–59. [CrossRef]

40. Cui, X.; Zhang, B.; Zeng, C.; Guo, S. Electrocatalytic activity of high-entropy alloys toward oxygen evolution reaction. *MRS Commun.* **2018**, *8*, 1230–1235. [CrossRef]

41. Kalimuthu, V.S.; Attias, R.; Tsur, Y. Electrochemical impedance spectra of RuO_2 during oxygen evolution reaction studied by the distribution function of relaxation times. *Electrochem. Commun.* **2020**, *110*, 106641. [CrossRef]

42. Joya, K.S.; Ehsan, M.A.; Babar, N.-U.-A.; Sohail, M.; Yamani, Z.H. Nanoscale palladium as a new benchmark electrocatalyst for water oxidation at low overpotential. *J. Mater. Chem. A* **2019**, *7*, 9137–9144. [CrossRef]

43. Highfield, J.; Claude, E.; Oguro, K. Electrocatalytic synergism in Ni/Mo cathodes for hydrogen evolution in acid medium: A new model. *Electrochim. Acta* **1999**, *44*, 2805–2814. [CrossRef]

44. Shervedani, R.K.; Madram, A.R. Kinetics of hydrogen evolution reaction on nanocrystalline electrodeposited $Ni_{62}Fe_{35}C_3$ cathode in alkaline solution by electrochemical impedance spectroscopy. *Electrochim. Acta* **2007**, *53*, 426–433. [CrossRef]

45. Plata-Torres, M.; Torres-Huerta, A.; Domínguez-Crespo, M.; Arce-Estrada, E.; Ramírez-Rodríguez, C. Electrochemical performance of crystalline Ni–Co–Mo–Fe electrodes obtained by mechanical alloying on the oxygen evolution reaction. *Int. J. Hydrogen Energy* **2007**, *32*, 4142–4152. [CrossRef]

46. Hanumantrao, S.S.; Haram, S.K. Kinetic Analysis of the Oxygen Evolution Reaction (OER) Performed with a Cobalt-Phosphate Electrocatalyst. *Chem. Sel.* **2017**, *2*, 3323–3328.